Pergamon

Scripta Materialia, Vol. 39, No. 9, pp. 1317–1323, 1998
Elsevier Science Ltd

1359-6462/98 $19.00 + .00

PII S1359-6462(98)00291-7

TEXTURE DEVELOPMENT AND TRANSFORMATION STRAIN OF A COLD-ROLLED Ti50-Ni45-Cu5 ALLOY

L. Zhao, P.F. Willemse, J.H. Mulder[#], J. Beyer and W. Wei*
University of Twente, Faculty of Mechanical Engineering, Materials Science and Engineering Group, P.O. Box 217, NL-7500 AE Enschede, The Netherlands

(Received June 16, 1998)
(Accepted June 30, 1998)

1. Introduction

Shape memory alloys (SMAs) are finding increased use as functional materials in the aerospace, energy and medical industries (1–3). Shape memory behaviour is based on the recovery of large amounts of induced strain upon heating and/or unloading. This transformation strain is a result of the reversible growth of certain favoured martensite variants during martensite transformation and/or stressing [4–5]. For single crystal SMAs, the favoured variants are those which result in the maximum transformation strain for a specific orientation. This has been well established for several common single crystal SMAs such as TiNi, CuZnAl and CuAlNi [4,6].

For polycrystalline SMAs, it is not clear which variants are favoured. Anisotropic behaviour in SMAs has been interpreted based on the anisotropy data of single crystal materials using the concept of the selection of favoured martensite variants. This has met with only limited success in work on NiTi alloys due to the lack of information about which variants are formed [7–8]. An investigation of the anisotropic behaviour of textured SMAs was thus conducted in order to determine which martensite variants develop during thermal cycling of a commercial TiNiCu SMA. The relationship between the observed variant development, changes in texture and anisotropic shape memory behaviour are discussed in light of models using the concept of favoured martensite variants.

2. Experimental

This work was conducted on a Ti50Ni45Cu5 (at.%) SMA supplied by n.v. AMT, Belgium. The material was received in sheet form, annealed at 800°C for 1 h in a vacuum furnace and then cold-rolled from 4.3 mm down to 0.8 mm in several steps at room temperature with intermediate anneals at 500°C for 10 min. The final thickness reduction after the last intermediate anneal was 19% and was followed by a final anneal at 500°C for 1.5 h to obtain high transformation strains. The transformation temperatures as determined by differential scanning calorimetry were M_S (martensite start) 56.9°C, M_f (martensite finish) 41.8°C, A_S (austenite start) 61.9°C, and A_f (austenite finish) 83.6°C.

#Present address: Hollandse Signaalapparaten B.V., P.O. Box 42, 7550 GD Hengelo, The Netherlands.
*Address correspondence to Prof. Dr. Wei.

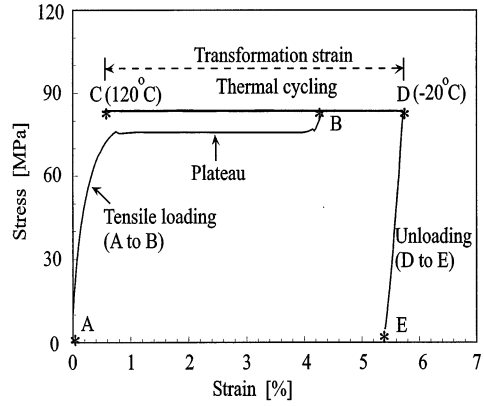

Figure 1. Example of the loading and thermal cycling process (sample cut 30° to RD).

Samples for tensile loading and texture measurements were spark-cut at angles of 0°, 30°, 45°, 60° and 90° to the rolling direction (RD), with sample dimensions of 45 × 15 × 0.9 mm. Textures were measured before and after thermal cyclic testing using a Philips X'pert system with CoKα radiation operating at 40 kV/30 mA. Austenite textures of the $\{110\}_p$, $\{200\}_p$ and $\{211\}_p$ diffractions planes were measured at 120°C using a heating stage. Orientation distribution functions (ODF) for quantitative analysis of the austenite texture and inverse pole figures were calculated by a Philips ODF program. Pole figures were also measured for the $(002)_m$, $\{11\bar{1}\}_m$, $(020)_m$, $\{111\}_m$ and $(022)_m$ monoclinic martensite diffraction planes.

Thermal cyclic testing was conducted using the procedure shown in Fig. 1. The samples were loaded to a stress 10% above the plateau stress (pts. A to B) in a Zwick tensile testing machine. The stress levels as a function of angle to the RD are given in Table 1. The specimens were then thermally cycled once between −20°C (pt. D) and 120°C (pt. C) at a rate of 0.167° C/s under the given constant stress. The transformation strains (C-D) were determined using an MFS mini strain gauge with a gauge length of 10 mm. The samples were then unloaded (pt. E) and the resulting martensite textures measured.

3. Results

3.1 Anisotropic Behaviour of Transformation Strain

The results of thermal cyclic testing showed an angular dependence of the transformation strain. The strain was 5.04–5.13% at angles of 0° to 45° to the RD, decreasing to 2.80% in the TD (see curve marked ε_{exp} in Fig. 4). The anisotrophy parameter (ratio of maximum to minimum values of the transformation strain) is thus equal to about 1.8 which agrees with that measured by Monasevich et al (8) after thermal cyclic testing of a hot-rolled Ti-50Ni alloy under a constant stress of 50 MPa.

TABLE 1
Constant Loads used for Thermal Cyclic Testing.

Angle to RD (°)	Stress level (MPa)	Angle to RD (°)	Stress level (MPa)
0	86	60	90
30	80	90	140
45	84		

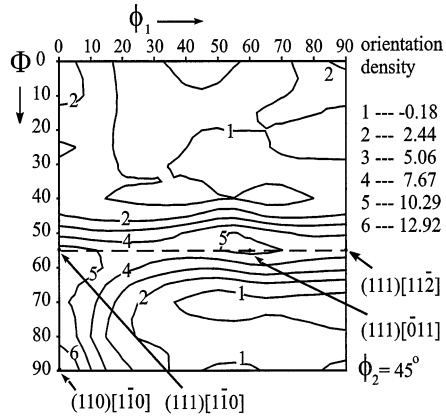

Figure 2. ODF section of the austenite phase at $\Phi_2 = 45°$ for an as cold-rolled and heat treated sample.

3.2 Texture Development

An ODF section of the austenite texture at $\phi_2 = 45°$ shows that the texture consists of $(110)[1\bar{1}0]_p$ and $(111)[1\bar{1}0]_p$ components, see Fig. 2. The $\{110\}<1\bar{1}0>_p$ component is sharp, and its orientation density decreases considerably on departing from the exact $(110)[1\bar{1}0]_p$ orientation, $\Phi = 90°$, $\phi_1 = 0°$. The density of the $\{111\}<1\bar{1}0>_p$ component is lower than that of $\{110\}<1\bar{1}0>_p$, with the density variation along the line $\Phi = 55°$ being small, resembling a $\{111\}<uvw>_p$ fibre texture. The $\{110\}<1\bar{1}0>_p$ component can thus be regarded as the main texture component.

Thermal cycling resulted in changes in the as-transformed martensite texture. $\{11\bar{1}\}_m$ pole figures before and after thermal cyclic testing in the 0° and 45° directions are shown in Fig. 3. The textures were analyzed using stereographic projections calculated using the lattice parameters of the monoclinic TiNi alloy: a = 0.2889 nm, b = 0.4120 nm, c = 0.4622 nm, and $\beta = 96.8°$ (9). The texture could only be analyzed up to a tilt angle of 70° because information at higher tilt angles was less reliable due to defocussing effects [10].

Before loading, four martensite texture components, *viz.* $(002)[020]_m$, $\{111\}<2\bar{1}1>_m$, $\{020\}<002>_m$ and $\{11\bar{1}\}<2\bar{1}1>_m$ were found (Fig. 3a). These four components include all 12 variants originating from the $\{110\}<110>_p$ austenite texture as given by Miyazaki, et al [4], Table 2. The presence of minor texture components originating from the $\{111\}<1\bar{1}0>_p$ component can be seen by the shift and spread of the intensity contours. The 3' variant originating from the $\{111\}<1\bar{1}0>_p$ component apparently causes the elongation of the contours and the shift of the maximum intensity away from the marked component positions (see arrows in Fig. 3a). The pole figures for loading along the transverse direction (TD) resemble the pole figures before thermal cycling, indicating that all 12 variants may still be present. Because a finite amount of transformation strain was measured, the relative amount of these variants must have changed. It was, however, difficult to observe these relative changes in the pole figures.

Figs. 3bc show that the martensite texture is dependent on loading direction. In the RD, six variants (1′, 2′, 3, 4′ and 5, 5′, see Table 2) are formed, as demonstrated by the weak intensity in the centre of the $\{11\bar{1}\}_m$ pole figure, Fig. 3b, as well as of the $\{111\}_m$ pole figure (not shown). The other 6 variants disappear as a result of the growth of favoured variants. At 45° the intensities in the second and fourth quarter become very weak while those in the first and third quarter remain high (Fig. 3c). This indicates that variant 5 becomes more dominant than 5', along these two variants give rise to the same texture

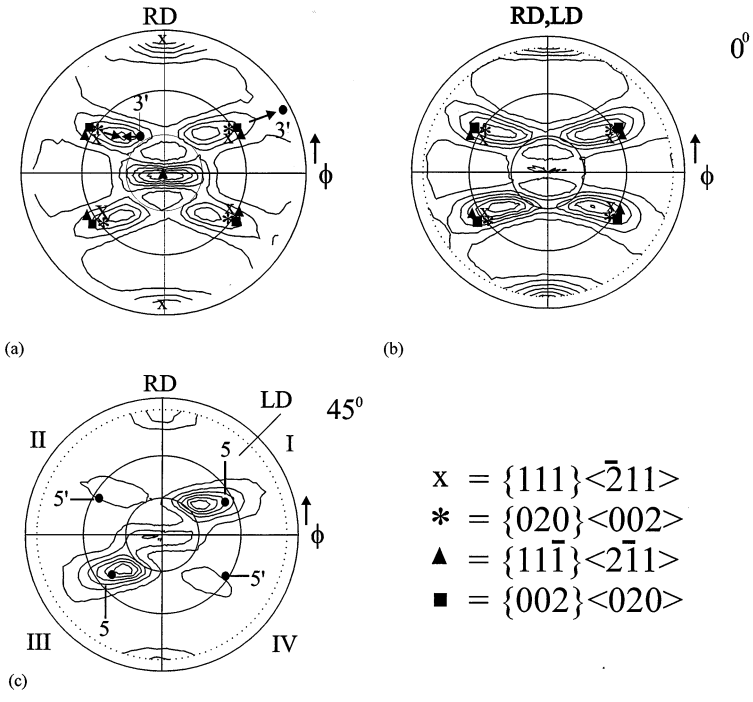

Figure 3. Pole figures of the $\{11\bar{1}\}$ martensite diffraction plane a) before testing, b) and c) after thermal cyclic testing at 0° and 45° to the RD. The Roman numerals indicate the quarters and the numbers indicate the variant number. RD = rolling direction, LD = loading direction.

component $\{020\}<002>_m$. The remaining variants were found to be 1′, 4′ and 5. The pole figures for loading 30° and 60° to the RD are similar to those for 45°.

4. Discussion

The results of this investigation show that the transformation strain during thermal cyclic testing under constant load is a function of the angle between the loading and rolling directions. The transformation strain between 0° and 60° is relatively constant but then decreases significantly towards the TD. It was found that the martensite texture which develops during testing is also a function of angle and the

TABLE 2
Calculated Martensite Variants Originating from the $(110)[1\bar{1}0]_p$ and $(111)[1\bar{1}0]_p$ Austenite Texture using the Notation of Correspondence Variants from Miyazaki et al. [4].

Variant	$(110)[1\bar{1}0]_p$	$(111)[1\bar{1}0]_p$	Variant	$(110)[1\bar{1}0]_p$	$(111)[1\bar{1}0]_p$
1	$(\bar{1}11)[2\bar{1}1]$	$(\bar{1}20)[2\bar{1}1]$	4	$(11\bar{1})[\bar{2}1\bar{1}]$	$(10\bar{2})[\bar{2}1\bar{1}]$
1′	$(\bar{1}11)[\bar{2}11]$	$(\bar{1}20)[\bar{2}11]$	4′	$(\bar{1}11)[2\bar{1}1]$	$(\bar{1}02)[2\bar{1}1]$
2	$(\bar{1}11)[211]$	$(\bar{1}02)[211]$	5	$(020)[00\bar{2}]$	$(\bar{1}20)[00\bar{2}]$
2′	$(\bar{1}11)[\bar{2}11]$	$(102)[\bar{2}11]$	5′	$(020)[00\bar{2}]$	$(\bar{1}20)[00\bar{2}]$
3	$(111)[\bar{2}11]$	$(\bar{1}20)[\bar{2}11]$	6	$(002)[0\bar{2}0]$	$(10\bar{2})[0\bar{2}0]$
3′	$(\bar{1}11)[2\bar{1}1]$	$(\bar{1}20)[2\bar{1}1]$	6′	$(002)[020]$	$(\bar{1}02)[020]$

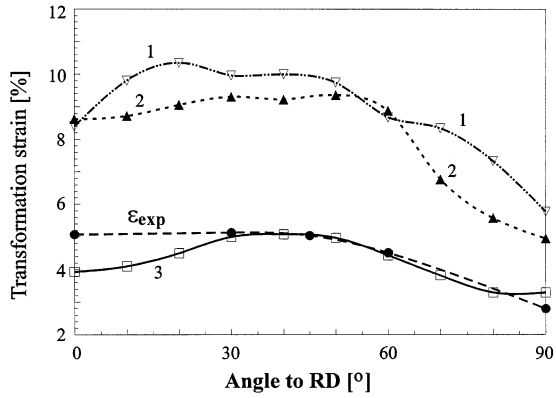

Figure 4. Comparison between the experimentally measured transformation strains ε_{exp}, and strains calculated by 1) maximum transformation strain from a mixed texture of $(110)[110]_p$ and $(111)[110]_p$ components, 2) average transformation strain from two groups of variants, 3) Taylor model accounting for mutual constraint between grains in polycrystalline material.

variant selection at each angle. Given that different martensite variants can lead to different transformation strains [e.g. 11–12], a number of models based on texture components were used to try to reproduce the experimentally measured strains based on the measured data. The results of these calculations are shown as curves 1–3 in Fig. 4.

Curve 1 was calculated based on single crystal data. This calculation considers both austenite components $\{110\}\langle 1\bar{1}0\rangle_p$ and $\{111\}\langle 1\bar{1}0\rangle_p$ and the anisotropy is calculated using a rule of mixtures, where the $\{110\}\langle 1\bar{1}0\rangle_p$ component contributes 55% of the maximum strain and the $\{111\}\langle 1\bar{1}0\rangle_p$ component 45%, as estimated from the relative densities of these components in the ODF section, see Fig. 2. In Fig. 4 it can be seen that the calculated curve lies significantly higher than the experimental results. However, the anisotropy parameter (1.80) is the same as that of the measured one.

The texture measurements show, however, that more than one variant formed during thermal cycling. The formation of martensite under stress requires the simultaneous nucleation and growth of several variants, whereas in a single crystal only the variant with the maximum strain results. Calculations were therefore made considering the strain contributed by all variants found in the measured textures. First, the transformation strains associated with variants originating from the $\{110\}\langle 1\bar{1}0\rangle_p$ were calculated and classified according to the amount of strain. It was found that most of the transformation in a given direction is contributed by not one but two groups of variants, see Table 3, namely, the group of variants with the maximum strain in the loading direction and the group of variants with the second largest strains. The development of these two groups of variants arises from the necessity to fulfil the compatibility condition among grains. For instance, in a single crystal only variant 5 is developed in the $[11\bar{1}]_p$ direction, while for polycrystalline material, variants 1′ and 4′ are also found for the angle 30° to the RD.

The anisotropy of transformation strain was subsequently calculated by using these two groups of variants. The amount of each variant formed was based on the density of the inverse pole figure and it was assumed that variant(s) with compressive transformation strain(s) along the tensile loading direction would not contribute. The strains in each direction are thus the averages of the strains of the variants formed in that direction, whereby the strain, ε_y' in the loading direction is given as

$$\varepsilon_y' = \frac{R_y\langle 100\rangle \cdot \varepsilon_y\langle 100\rangle + R_y\langle 110\rangle \cdot \varepsilon_y\langle 110\rangle + R_y\langle 111\rangle \cdot \varepsilon_y\langle 111\rangle}{R_y\langle 100\rangle + R_y\langle 110\rangle + R_y\langle 111\rangle} \quad (1)$$

TABLE 3
Calculated Transformation Strain (%) of the Correspondence Variants in NiTi Alloys. The Number in Parentheses is the Number of the Variant According to Miyazaki, see Table 2.

Angle to RD	0°	30°	45°	60°	90°
			For $(110)[1\bar{1}0]_p$		
largest strain	8.40	10.33	10.03	8.91	2.68
	(5,5′)	(5)	(1′,4′)	(1′,4′)	(1,1′,2,2′,3,3′,4,4′)
second largest strain	3.60	9.35	8.15	4.35	−4.18
	(1′,2′,3,4′)	(1′,4′)	(5)	(5)	(5,5′,6,6′)
			For $(111)[1\bar{1}0]_p$		
largest strain	8.40	9.50	9.93	8.40	9.50
	(3,3′)	(3′,5)	(5)	(5,5′)	(1,5′)
second largest strain	3.60	5.82	7.22	3.60	5.82
	(1′,2′,5′,6)	(2′)	(3′)	(1′,2′,3′,4)	(4)

where ε_y' = mean strain in the loading (y) direction, ε_y = calculated strain in a single crystal in the direction <uvw>, and R_y = density of the inverse pole figure in the direction <uvw>.

These calculated transformation strains are shown as curve 2 of Fig. 4. The calculated strains of curve 2 are closer to the experimental strain in the RD and TD than curve 1, but are still too high at the intermediate angles.

To further improve the calculation, a model proposed by Ono (13) was thus used in which the calculated transformation strains for single crystals can be modified by a Taylor factor M′ in which the effect of the mutual strain constraint between grains is included. Use of this approach results in curve 3 of Fig. 4. This curve fits the experimental data the best with a slight discrepancy close to the RD. This discrepancy may arise for a number of reasons. Minor martensite texture components originating from the $\{111\}<110>_p$ component were not separated in the pole figures because they are overlapped by the major texture components. The minor components could not be determined by analysis of texture using an ODF calculation, which is still under development for the monoclinic lattice. Factors such as dislocation density, grain size and grain shape which can significantly influence the transformation strain, were also not taken into account. Work is continuing to improve these calculations.

5. Conclusions

Texture development and anisotropic shape memory behaviour of a cold-rolled Ti50-Ni45-Cu5 shape memory alloy during thermal cycling under constant load were determined. It was found that the martensite texture after thermal cycling was dependent on the types of variants which developed. In contrast to single crystals, those martensite variants showing the two largest transformation strains in the loading direction developed. The relationship between texture development and transformation strain, and the transformation strains as a function the angle between the loading direction and the RD can be predicted based on those variants. It was found that a Taylor model was most suited for the calculation of transformation strains.

Acknowledgments

This research was supported by the Dutch Technology Foundation (STW). The authors are grateful to Prof. H. Bunge and Mr. W.Q. Yuan from the Technical University of Clausthal, for their assistance with

ODF calculations and in the confirmation of texture measurements, and Dr. M. Chandrasekaran (n.v. AMT, Belgium) for valuable discussions.

References

1. J. van Humbeeck, Shape Memory Materials and Phenomena—Fundamental Aspects and Applications, p. 3771, vol. 246, MRS, Pittsburgh, PA (1992).
2. C.M. Wayman, J. Metals. June, 129 (1980).
3. C. Boller, ed., Smart Structures and Materials: Implications for Military Aircraft of New Generation, AGARD Lecture Series 205, AGARD, Neuilly-sur-Seine, France (1996).
4. S. Miyazaki, K. Otsuka, and C.M. Wayman, Acta Metall. 37, 1873 (1989).
5. K. Otsuka, Mater. Sci. Forum 56–58, 393 (1990).
6. J. Perkins, Mater. Sci. Eng. 51, 181 (1981).
7. J.H. Mulder, P.E. Thoma, and J. Beyer, Z. Metallkd. 84, 501 (1993).
8. L.A. Monasevich, Yu I., Paskal, V.E. Prib, G.D. Timonin, and D.B. Chernov, Metalloved. Term. Obrab. Met. 9, 62 (1979).
9. K. Otsuka, T. Sawamura, and K. Shimizu, Phys. Stat. Sol. (a). 5, 457 (1971).
10. E.M.C. Huijser-Geriis and G.D. Rizek, J. Appl. Crystlog. 7, 286 (1974).
11. T. Saburi and S. Nenno, in on Solid-Solid Phase Transformation, p. 1455, TMS of AIME, Warrendale, PA (1982).
12. P. Cizek, Kovove Materialy. 27, 1, 98 (1989).
13. N. Ono, A. Sato, and H. Ohta, Materials Trans. JIM. 30, 756 (1989).